ACS APPLIED MATERIALS & INTERFACES

Article

Novel Integration of Perovskite Solar Cell and Supercapacitor based on Carbon Electrode for Hybridizing Energy Conversion and Storage

Zhiyong Liu, Yan Zhong, Bo Sun, Xingyue Liu, Jinghui Han, Tielin Shi, Zirong Tang, and Guanglan Liao

ACS Appl. Mater. Interfaces, **Just Accepted Manuscript** • DOI: 10.1021/acsami.7b01471 • Publication Date (Web): 14 Jun 2017

Just Accepted

ACS Publications

ACS Applied Materials & Interfaces is published by the American Chemical Society.
1155 Sixteenth Street N.W., Washington, DC 20036

Novel Integration of Perovskite Solar Cell and Supercapacitor based on Carbon Electrode for Hybridizing Energy Conversion and Storage

Zhiyong Liu†[a], Yan Zhong†[a], Bo Sun[a], Xingyue Liu[a], Jinghui Han[a], Tielin Shi[a], Zirong Tang[a] and Guanglan Liao*[a,b]

[a] *State Key Laboratory of Digital Manufacturing Equipment and Technology, Huazhong University of Science and Technology (HUST), Wuhan 430074, China*

[b] *Flexible Electronics Research Center, Huazhong University of Science and Technology, Wuhan 430074, China*

** Address correspondence to (G. Liao) guanglan.liao@hust.edu.cn.*

† Zhiyong Liu and Yan Zhong contributed equally to this work.

Abstract

Power packs integrating both photovoltaic parts and energy storage parts have gained great scientific and technological attention due to the increasing demand for green energy and the tendency for miniaturization and multi-functionalization in electronics industry. In this study we demonstrate novel integration of perovskite solar cell and solid-state supercapacitor for power packs. The perovskite solar cell is integrated with the supercapacitor based on the common carbon electrodes to hybridize photoelectric conversion and energy storage. The power pack achieves a voltage of 0.84 V when the supercapacitor is charged by the perovskite solar cell under the AM 1.5G white light illumination with a 0.071 cm^2 active area, reaching an energy storage proportion of 76% and an overall conversion efficiency of 5.26%. When the supercapacitor is pre-charged at 1.0 V, an instant overall output efficiency of 22.9% can be achieved if the perovskite solar cell and supercapacitor are connected in series. These exhibit great potential in the applications of solar energy storage and flexible electronics such as portable and wearable devices.

Keywords: perovskite solar cell, carbon electrode, supercapacitor, power pack, integration

1. Introduction

There is an increasing demand for green energy and a tendency for miniaturization and

multi-functionalization in electronics industry. As for green energy, organometal perovskites have exhibited considerable prospects as next generation photovoltaics due to their unique properties, including ideal absorption-appropriate[1, 2] and adjustable bandgap[3-6], high absorption coefficient[7], long carrier diffusion length[8], bipolar transport[9] and high tolerance of chemical defects[10-12]. By immersing into burgeoning researches into the field of perovskite photovoltaics, perovskite solar cells (PSCs) have achieved power conversion efficiencies (PCE) rapidly approaching 22.1%, exhibiting incredible momentum of development and potential value for application. From their humble beginnings, pervoskite-based photovoltaics are now leading the pack of emerging solar technologies, *e.g.* dye-sensitized solar cells, organic thin-film solar cells and quantum dot solar cells. Moreover, considering the cost and stability of the PSCs, printable carbon counter electrode based hole-conductor-free PSCs, which possess a far lower energy payback time than the traditional silicon photovoltaic devices, have been proven to be one of the most promising photovoltaic devices[13-18]. PSCs equaling to other photovoltaic devices have to be applied in sunlight (usually intermittent and unpredictable) to generate electric energy. Their PCEs are dependent on the time, location, and weather. In order to alleviate these problems, it would be better to integrate the PSCs with energy storage devices to build power packs storing the electric energy generated by the PSCs. Supercapacitors (SCs) are excellent choices for the power packs, which are widely recognized as a new generation of clean energy-storage devices owing to their high power density, fast charge-discharge rate, long cycling life, and good operational safety[19-25]. The integrated energy system can convert and store the energy captured from the environment, providing a stable power output by mitigating transients caused by light intensity fluctuation or diurnal cycles and ensuring continuous work regardless of the availability of sunlight. The stored energy can then be released as and when required.

Much attempts have been made to integrate the energy conversion and storage devices into individual units for highly-efficient, light-weight and portable devices[26-32]. Zou *et al*[33] and Liu *et al*[34] introduced a self-powering energy power fiber that incorporated a dye-sensitized solar cell and a SC to hybridize energy conversation and storage. Wang *et al.* and Gong *et al*. presented investigations on power packs combining PSCs with SCs through external wires or power management circuit and evaluated their performance as energy packs[35, 36]. Thereafter, an individual integrated device based on printable PSCs with the dual function of solar-electricity and

supercapacitive energy storage was also reported, delivering a maximum efficiency up to 4.7% with an energy storage efficiency of 73.77%.[37] Zhou *et al.* demonstrated co-anode and co-cathode photovoltachromic SCs which were potential for multifunctional smart window applications.[38] However, the structures of those integrated systems are still rigid, and investigations on the power packs are still inadequate.

In this study, we propose a novel integration method for the power packs. The fabrications of carbon counter electrode based PSCs and MnO_2 asymmetric solid-state SCs (ASCs) are investigated. Then we integrate the PSC with the SC based on the common carbon electrode for hybridizing photoelectric conversion and energy storage. The SCs can be charged by the PSCs under the AM 1.5 white light illumination and the stored energy can be used to drive loads. When the two components are integrated and connected in series, the instant output of the solar cell is strengthened. These demonstrate that the power packs have great potential in the applications of flexible electronics such as portable and wearable devices.

2. Results and discussion

The schematic of the carbon counter electrode based printable mesoscopic PSC is presented in Figure 1a. Both of the compact TiO_2 layer and the mesoscopic TiO_2 layer are prepared by spin-coating method. The $CH_3NH_3PbI_3$ perovskite light absorber layer is deposited by the sequential method[39]. The carbon layer as the counter electrode of the solar cell is directly printed on the perovskite layer by doctor-blade method. Photo-generated holes transport to the counter electrode since halide perovskites can act as a hole conductor as well. Figure 1b presents the cross section scanning electron microscopy (SEM) images of the carbon counter electrode based PSC. The thickness of the TiO_2 layer is approximately 600 nm. Perovskite capping, inserted between the carbon layer and TiO_2 layer with a thickness of ~500 nm, can prevent direct contact between the photo-anode and back electrode. As shown in Figure 1c, we obtain uniform, dense, and full-coverage perovskite films with large grain size. The roughened interface will also strengthen internal light scattering. The formation of $CH_3NH_3PbI_3$ is confirmed by the EDX spectroscopys as shown in Figure S1. Strong diffraction peaks at 14.01, 19.94, 23.44, 24.46, 28.38, 31.8, 40.46 and 43.06 are derived from the (110), (112), (211), (202), (220), (310), (224) and (314) planes of the tetragonal perovskite structure[40, 41], as shown in Figure 1d. The photocurrent density-photovoltage

(*J-V*) curves of the PSC under standard AM 1.5G illumination at 100 mW cm^{-2} are displayed in Figure 1e. The optimal cell achieves a PCE of 7.79 %, a V_{OC} of 0.96 V, a J_{SC} of 15.7 mA cm^{-2}, and a FF of 0.52 when measured under a reverse voltage scan. In order to avoid overestimating the conversion efficiency from the hysteresis effect, which depends on the scan direction and scan rate, both the forward and reverse bias sweep are used to evaluate the hysteresis behavior of the PSC. As shown in Figure S2, our device exhibits a negligible hysteresis and efficiency fluctuation, although the hysteresis effect become a little obvious with the increment of the scan rate, which is mainly embodied in the change of FF. Figure 1f shows the incident photon-to-current conversion efficiency (IPCE) over the spectral range from 300 to 800 nm. Integration of the IPCE spectrum over the solar emission yields AM 1.5 photocurrents of 15.8 mA cm^{-2} for the device, in excellent agreement with the measured J_{SC} value.

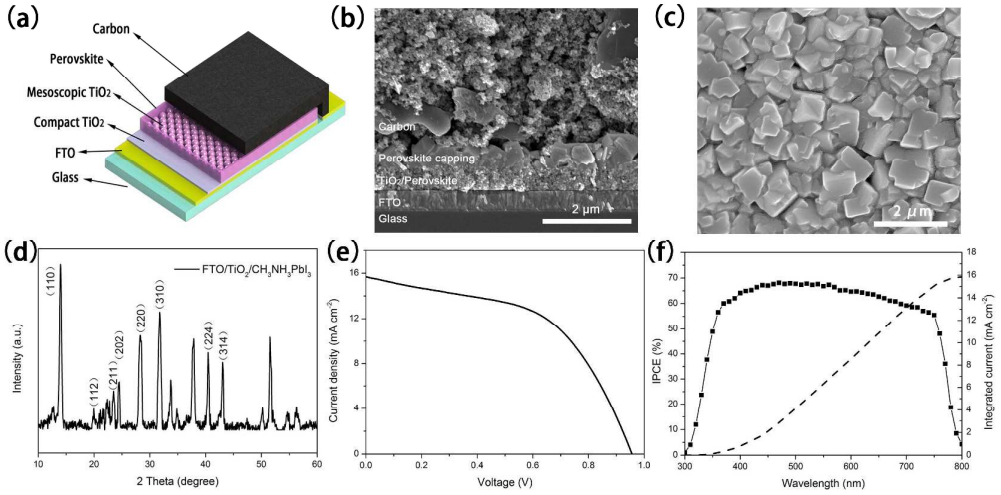

Figure 1. (a) The schematic structure of the carbon counter electrode based PSC; (b) Cross-sectional SEM image of the PSC; (c) SEM images of the perovskite layer prepared by a two-step method; (d) XRD spectrum of $CH_3NH_3PbI_3$; (e) Photocurrent density-voltage (*J-V*) characteristics of the PSC; (f) The corresponding IPCE of the PSCs and the integrated current calculated from the overlap integral of the IPCE spectra.

Graphite sheet, benefiting from its high conductivity and excellent flexibility, is chosen as the substrate for the SC part. Mesoporous carbon film, prepared by the screen-printing method, is used as the negative electrode for the SC. The SEM photographs and electrochemical performance of the mesoporous carbon film is shown in Figure S3b and Figure S6. MnO_2, one of the most

promising electrode materials for faradaic pseudo-capacitors, is used as the positive electrode in the asymmetric SC and prepared by electrochemical deposition. As shown in Figure S3d, the high magnified SEM exhibits the rough surface of MnO_2, which possesses high surface area for more ion absorption and enhanced capacitance. XPS studies are also conducted to verify the formation synthesis of MnO_2 on the carbon film (Figure S4).

To evaluate the performance of the SC, the electrochemical properties are characterized by cyclic voltammetry (CV) and galvanostatic discharging method. Figure 2a shows the CV curves of the SC with various scan rates (from 0.01 V/s to 0.1 V/s). The rectangular shape for different scan rate indicates a high electrochemical stability and capacitance. Figure S5 also displays the CV curves of the positive and negative electrode at a san rate of 100 mV/s. Figure 2b shows the galvanostatic charge-discharge (GCD) curves with different current densities. The typical symmetrical triangular curve with little voltage drop confirms that the device has good capacitive performance. The area-specific capacitance *vs.* discharge current density is plotted in Figure 2c. As can be found, the areal capacitance of the SC device achieves 61.01 mF cm^{-2} and 46.46 mF cm^{-2} at the current density of 0.25 mA cm^{-2} and 1.0 mA cm^{-2}, higher than those reported in similar SCs[42-46]. Moreover, the area capacitance retains 64.3% of the initial value at a high current density (2.0 mA cm^{-2}) discharge, showing a good rate capability. The excellent capacitance and rate-capability of the SC are attributed to their unique structural features: (1) the highly conductive graphite paper enhances the efficient ion and electron transfer; (2) the MnO_2/carbon composites facilitate the cation diffusion between the electrolyte and electrode and help to overcome the poor electrical conductivity of MnO_2; (3) the LiCl/PVA electrolyte ensures the fast ion transport. It is worthy pointing out that the working potential of the assembled device can be expanded to 2.0 V in the gel electrolyte, as shown in Figure 2d. Figure 2e shows the GCD curves of a single device and a pair of devices connected in series. The connected pair can operate reversibly between 0 and 2.0 V. Long cycling life is important for SCs. The cycling life test over 5000 cycles for the SC is carried out by repeating the GCD test between 0 and 1.0 V at a current density of 2 mA cm^{-2}. Figure 2f exhibits a good cycling stability of the SC device. The capacitance decreases slightly with the retention of 96.2% after 5000 cycles, higher than those reported in other MnO_2-based SCs[47-49], showing great potential in energy storage devices. This is attributed to the stable electron

transport benefited from a good charge balance using the over potential of the two electrodes, a good adhesion between the carbon film and graphite paper, as well as the stable structure of the MnO_2/carbon composites. The leakage current of the as-fabricated device, about 100 μA after 500 s from the start and then stable for a long time beyond 2 h, is very small (Figure S7).

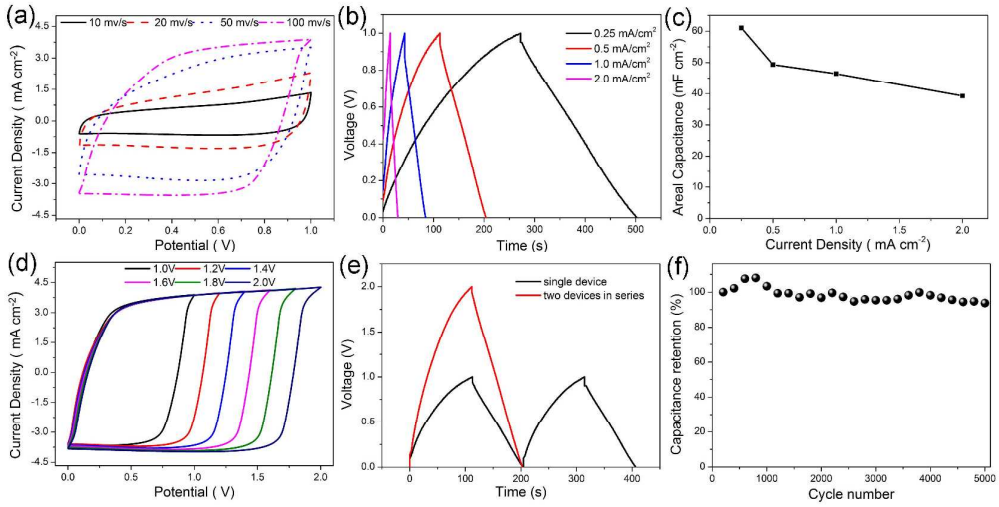

Figure 2. (a) CV curves of the SC under different scan rates in a two-electrode system; (b) GCD curves of the SC at different charge-discharge current densities; (c) Plot of the area-specific capacitance and discharge current density; (d) CV curves of the SC over different voltages at a scan rate of 100 mV s^{-1}; (e) GCD curves of a combing device in series at 0.5 mA/cm^2; (f) Cycle performance of the SC with a voltage of 1.0 V at a current density of 4.0 mA cm^{-2}

Then the PSC is integrated with the SC based on a carbon electrode for self-powered electronics to hybridize photoelectric conversion and energy storage (a co-anode system). Here the two components are connected in parallel (Figure 3a). Energy generated by the PSC can be stored in the SC and then released as needed. Since the carbon electrodes, which own the merits of easy molding and room-temperature fabrication[39, 50, 51], are employed both in the PSC and SC devices, we assemble them vertically before drying the carbon counter electrode of the PSC and obtain a novel integrated power pack. The structural schematic is shown in Figure 3b, where *A* and *B* are the negative and positive electrodes for the integrated device. Figure 3c displays the cross-sectional SEM image, where the detailed PSC structure can be distinguished in the zoomed inset.

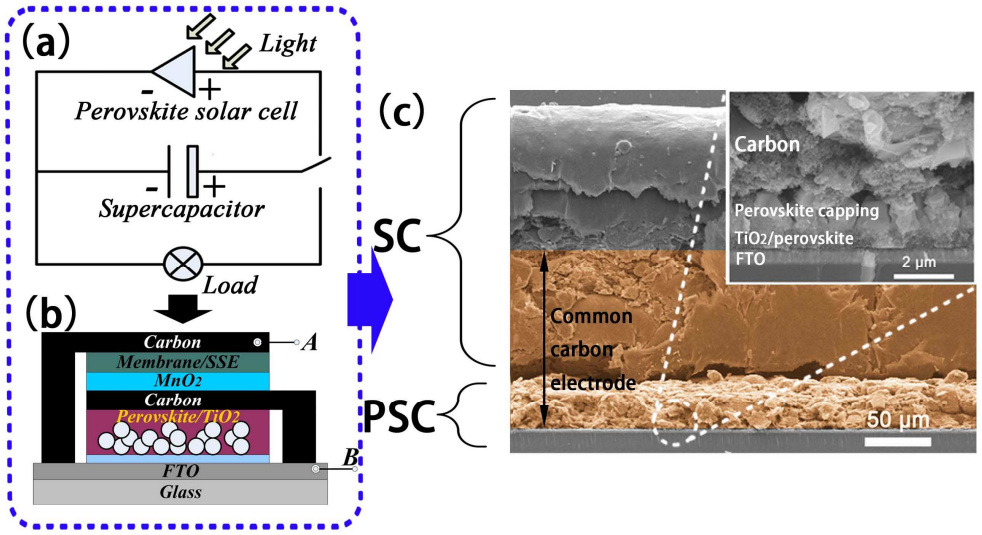

Figure 3. (a) Schematically diagram and (b) Structural schematic of the integrated device connected in parallel; (c) Cross-sectional SEM image of the integrated device; inset: the close-up of the PSC part.

Figure 4a depicts the real-time response of the photo-voltage for the power pack with the illuminated areas of 0.0314 cm^2, 0.071 cm^2, 0.124 cm^2 and 1.875 cm^2, respectively. When the integrated device is exposed to the irradiation of 1.0 sun, the voltage of the SC significantly increases at the beginning. Then the voltage increases slightly to a stable value when the device is further kept under illumination. The device with a larger active area, which can provide a larger photo-current, will significantly shorten the charging time and get a higher voltage for the capacitor part. Note that, the voltage plateau during the photo-charging process is lower than V_{OC} (0.96 V) of the PSC, which can be ascribed to the internal resistance.[34] The curves in Figure 4b show the trends of the energy storage proportion of the SC (χ) during the solar-charging process, similar to those in Figure 4a. The highest χ of 65%, 76%, 79% and 91% are acquired, corresponding to four kinds of active areas. In addition, Figure 4c presents the overall conversion efficiency of the integrated device ($\eta_{overall}$) during the solar-charging process. As the charging goes, the $\eta_{overall}$ gradually increases in the beginning and then decreases, and a peak can be obtained in the middle, which exhibits the overall performance of the power pack. The four peaks of $\eta_{overall}$ are calculated (4.32%, 5.26%, 3.97% and 1.27%, respectively), much higher than those reported integrated devices[30, 31, 33, 52]. The enhanced $\eta_{overall}$ may ascribe to the excellent photovoltaic property of the PSC and the compact structure of our novel integrated power pack. Particularly,

under the 0.071 cm^2 mask, the voltage of the SC has to be charged up to 0.70 V until we get a 5.26% efficiency. Thus, the maximum energy storage efficiency of the SC is calculated (η_{sc}=67.5%). Detailed calculation methods are provided in the experimental section. Figure 4d depicts the photo-charge/galvanostatic discharge curve of the power pack, demonstrating a good stability. The self-discharge curve is also obtained immediately after photo-charging to V_{max}, as shown in Figure 4e. The voltage difference between the two terminals of the power pack is recorded on an open circuit as a function of time. The degradation of the voltage mainly attribute to the self-consumption of the PSC. To evaluate the practical application of the power pack, a tandem system based on four individual devices (with an active area of 7.5 cm^2) is demonstrated: in the photo-charge process, the devices are connected in series; in the discharge process, a load is connected to the system. The results are shown in Figure 4f, where the photograph of the system is shown in the inset. The system can reach a stable output voltage of ~3.8 V within 15 seconds under the illumination of 1.0 sun, only a little lower than the V_{OC} of the PSCs. The assembled system is successfully used to drive LEDs after being photo-charged, lasting only several minutes due to the existence of self-energy consumption from the PSCs. Even so, this redundant consumption can be reduced by optimizing the individual PSC or SC and the integrating structures. These demonstrate the feasibility of the integrated power pack in hybridizing energy conversion and energy storage.

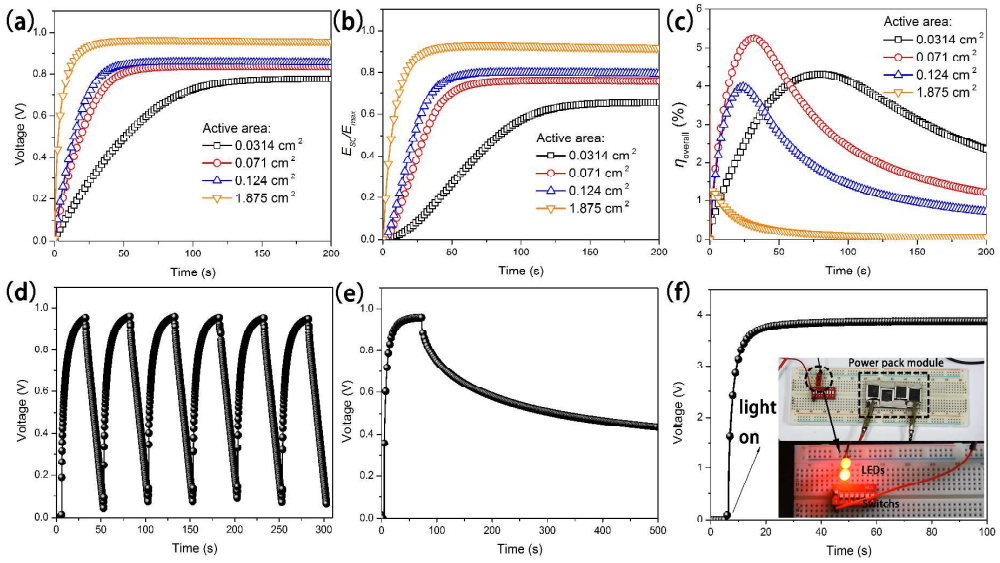

Figure 4. (a) Photo-charging curves of the power pack operated with illuminated areas of 0.0314 cm^2, 0.071 cm^2, 0.124 cm^2 and 1.875 cm^2; (b) the energy storage proportion (χ) of the SC part; (c)

overall energy conversion ($\eta_{overall}$) of the stored solar energy *versus* the solar-charging time; (d) photo-charging/galvanostatic-discharging curve of the power pack with an active area of 1.875 cm^2. The discharging current was set at 2.0 mA/cm^2. (e) photo-charging/self-discharging curve of the power pack. (f) solar-charging curve of a tandem system (four integrated devices connected in series with an active area of 7.5 cm^2). The photograph of the power pack is shown in the inset where the energy stored in the SC is used to drive LEDs.

Figure 5a depicts the integrated device in which the PSC and SC are connected in series, which can combine the advantages of PSC and SC and provide an instantaneous enhanced output power.[35] For example, V_{OC} of one single solar cell is limited (≈1V). After integrated with SC in series, we can obtain an enhanced V_{OC} (depending on the pre-charged SC). Fast charge-discharge property benefiting from the SC can also shorten the charge and discharge cycles, which may be meaningful in many electronic devices. As sketched in Figure 5b, the SC is turned upside down in the assembling, where *A'* and *B'* are used to pre-charge the SC, and *A'* and *C'* are applied for the output of the integrated device. Figure 5c presents the *J-V* characterization of the energy package when the SC is pre-charged at various voltages with the detailed parameters being tabulated in Table 1. The integrated device exhibits a rectification characteristic similar to the single solar cell, proving that the ion transport property in the SC will not affect the energy output of the PSC. The output currents of the system show a slight increment, and the output voltages almost equal to the sum of two individual devices. Noted that when the voltage of the SC is set at 1.0 V, the maximum output power of the integrated device can reach 22.9 mW cm^{-2} with an output voltage of 2.0 V, an output current of 21 mA cm^{-2}, and a fill factor of 0.55. Both the solar cell and capacitor contribute to the total electric power output. These results demonstrate a prototype of an integrated system for enlarged output power, exhibiting great potential for the application in self-powered electronic devices, *e.g.* sensors and actuators.

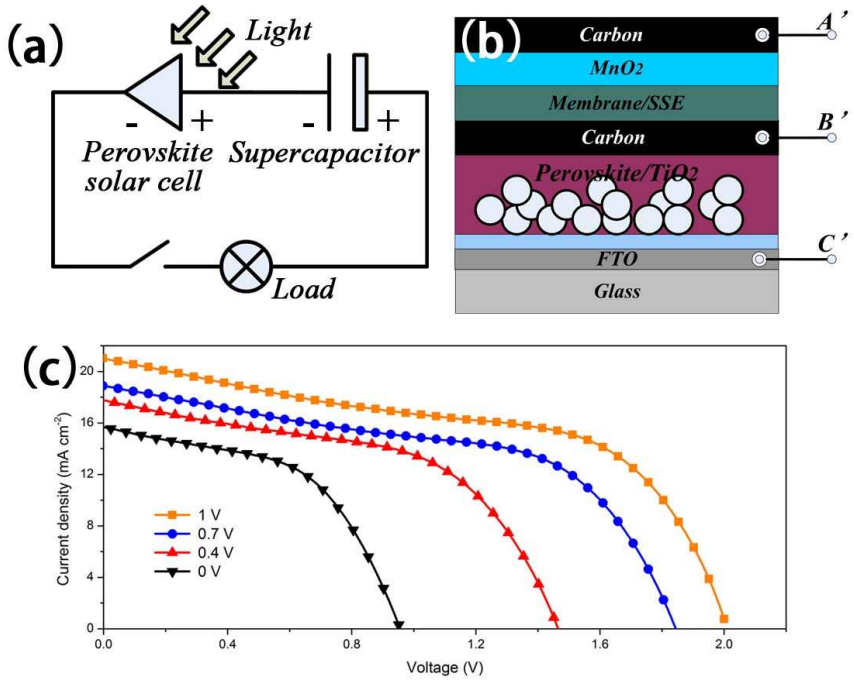

Figure 5. (a) Schematically diagram and (b) Structural schematic of the integrated device connected in series; (c) *J-V* curves of the integrated device when the SC was pre-charged to different potentials (0, 0.4, 0.7, and 1 V).

Table 1. Summary of the photovoltaic data averaged over 20 integrated energy packages under AM 1.5G irradiation by combining PSCs with SCs pre-charged at different voltages. The maximum data are included in the parentheses.

Potential of capacitor	V_{OC} (V)	J_{SC} (mA cm^{-2})	**FF**	P_{max} (mW cm^{-2})
0 V	0.93±0.03 (0.96)	14.2±1.5 (15.7)	0.50±0.02 (0.52)	6.6±1.2 (7.79)
0.4 V	1.38±0.08 (1.46)	16.2±1.6 (17.8)	0.50±0.03 (0.53)	11.2±2.5 (13.7)
0.7 V	1.74±0.10 (1.84)	17.2±1.6 (18.8)	0.51±0.03 (0.54)	15.3±3.4 (18.7)
1 V	1.90±0.10 (2)	18.9±2.1 (21)	0.53±0.02 (0.55)	19.0±3.9 (22.9)

3. Conclusion

The fabrication of carbon counter electrode based PSCs and MnO_2 asymmetric solid-state SCs is investigated. To hybridize the photoelectric conversion and energy storage, we propose a novel

power pack integrating the PSC with the SC based on a common carbon electrode, which can be used for self-powered electronics. The solid-state SC can be charged by the PSC under the AM 1.5G white light illumination. Illuminated with a 0.071 cm^2 active area, the power pack achieves a voltage of 0.84 V, reaching an energy storage proportion of 76% and an overall conversion efficiency of 5.26%. If connected in series, an overall output efficiency of 22.9% can be achieved when the SC is pre-charged at 1.0 V. These exhibit great potential in the applications of solar energy storage and flexible electronics, such as portable and wearable devices.

4. Experimental section

4.1. Synthesis of carbon paste

1 g polyvinyl acetate (the binder) and 0.5 g hydroxypropyl cellulose (the viscosity modifier) were dissolved in 60 ml ethyl acetate. Then 20 ml ethyl acetate solution was blended with 2 g 40 nm graphite powder, 1 g 10 μm flake graphite, 1 g 40 nm carbon black, 2g active carbon (YP-50F, purchased from Kuraray Chemical, Japan), and 0.5 g 50 nm ZrO_2 powder. The active carbon was used to improve the capacity of the SC. After vigorously milling for 2 h in a ball grinding machine (QM-QX0.4, Instrument Factory of Nanjing University), the carbon paste was ready.

4.2. Fabrication of the carbon counter electrode based PSCs

Fluorine-doped tin oxide substrates were firstly etched by zinc power and 2 M hydrochloric acid. Then the FTO substrates were ultrasonically cleaned by detergent, acetone, ethanol, and deionized (DI) water continuously. After treated with UV-ozone for 30 min, a 50 nm thick TiO_2 compact layer was deposited by spin-coating a mildly acidic solution of titanium isopropoxide in ethanol at a speed of 5000 rpm for 60 s, and annealed at 500 ^oC for 30 min. After cooling down to room temperature, the mesoporous TiO_2 nanocrystal film (particle size: 20 nm) was prepared by spin coating a commercial TiO_2 paste (DSL. 18NR-T, 20 nm, Dyesol, Australia) diluted in ethanol (2:7, weight ratio) at 5000 rpm for 60 s. The film was sintered at 500 ^oC for 30 min. The $CH_3NH_3PbI_3$ organic-inorganic perovskite layer was prepared by a two-step sequential method. Firstly, the PbI_2 mixed precursor solution (1.7 g PbI_2 in 2 ml N,N-dimethylformamide and 400 μl dimethylsulfoxide) was spin-coated on the TiO_2 porous film at 2000 rpm for 45s, followed by annealing at 70 ^oC for 10 min. Sequentially, the films were infiltrated by 2-propanol for 1-2 s

before being immersed in a solution of CH_3NH_3I in 2-propanol (10 mg ml^{-1}) for 15 min and then rinsed with 2-propanol. During the transferring process, the color of the films changed from light yellow to black, indicating the successful formation of perovskite layer. Finally, the films were dried at 70 ^oC for 10 min. The deposition of carbon CE was conducted by doctor blade method with the carbon paste. The whole process was accomplished at ambient condition.

4.3. Characterization of the PSCs

The *J-V* characteristics of the $CH_3NH_3PbI_3$-based solar cells were measured by an electrochemical station (Autolab PGSTAT302N, Metrohm Autolab, Utrecht, The Netherlands) under simulated AM 1.5 sunlight at 100 mW cm^{-2} irradiance generated by solar simulator (Oriel 94043A, Newport Corporation, Irvine, CA, USA). A Si reference cell (Newport Stratford), calibrated by the National Renewables Energy Laboratory, was used to calibrate the light intensity, where the mismatch factor was estimated to be 1%. The devices were tested by using a metal mask with an area of 0.1 cm^2. The IPCE was tested under illumination of monochromatic light from a xenon lamp coupled with a monochromator (TLS1509, Zolix). The perovskite surface and the cross-sectional structure of the solar cells was characterized with a field-emission scanning electron microscopy (FE-SEM, JSM-7600F, JEOL).

4.4. Fabrication of the solid-state SCs

Graphite sheet was chosen as the substrate due to its low cost, flexibility as well as its considerable conductivity. The mesoporous carbon film was prepared by doctor-blade method. MnO_2 electrode was obtained by galvanostatic electrochemical deposition on the carbon electrode in a 0.16 M $MnSO_4 \cdot H_2O$ aqueous solution. The reaction current density was set at 3.7 mA cm^{-2} and the deposition time was optimized at 3 min. After rinsed by DI water, the MnO_2 electrodes were dried in an oven at 45 ^oC. The PVA-LiCl solid-state electrolyte was prepared as follows: 1.696 g LiCl was added into 40 mL deionized water, and then 4 g PVA power was added. The mixture was heated steadily to 95 ^oC under vigorous stirring until the solution became clear. Then, the solution was allowed to stand at 95 ^oC for two hours to remove the residual bubbles. The solid-state SC was fabricated by immersing MnO_2 electrode and carbon electrode in the PVA-LiCl electrolyte for 5 min, respectively. Then two electrodes coated with solid-state electrolyte were

face-to-face assembled together with a piece of filter paper as the membrane. The device was kept at 45 ^{o}C for 12 h to ensure the complete solidification of the PVA-LiCl gel.

4.5. Characterization of the solid-state SCs

FE-SEM was carried out to investigate the film morphology of the graphite sheet, mesoporous carbon film and MnO_2 particles. Cyclic voltammetry (CV) was conducted on the electrochemical station and galvanostatic charge-discharge measurement were conducted by using a multichannel battery measurement system (Land, China). Both the CV measurement and galvanostatic charge-discharge measurement were carried out at the potential ranging from 0 to 1 V.

4.6. Fabrication of the power packs

The power packs were prepared by integrating PSCs and SCs in vertical direction and the two elements were connected in parallel or in series. Briefly, after printing the carbon counter electrode for the PSC, we pasted the pre-prepared asymmetric SC on the carbon film before its solidification. For the parallel connection, the MnO_2 electrode contacted with the carbon counter electrode was used as the positive electrode for the integrated device. For the series connection, the SC was turned upside down. After the carbon film was completely dried in a drying oven at 80 ^{o}C, the integrated device was finished. The SC was charged by the current generated from the PSC under white light illumination. The performance of the power pack was studied by the electrochemical workstation.

4.7. Calculations

The area-specific capacitance (C) of the SC can be obtained from the galvanostatic charge-discharge curves[33]

$$C=Q/(A\times\Delta V) =\int I\times dt/(A\times\Delta V)=I\times t_{discharge}/[A\times(V- I\times R_{drop})] \quad (1)$$

where I is the discharging current, $t_{discharge}$ is the discharging time, V is the highest voltage, R_{drop} is the voltage drop at the beginning of the discharge, and A is the effective surface area of the SC. The energy (E_{SC}) stored in the SC (C_{SC}) during the photo-charging process is calculated by[33]

$$E_{SC}=0.5C_{SC}\times V^2 \quad (2)$$

where C_{SC} is the capacitance of the SC, and V is the voltage of the SC. The maximum voltage of the SC can reach the value of V_{OC} in an ideal mode. Therefore, the maximum energy stored in the SC (E_{max}) is equal to $0.5C_{SC}\times V_{OC}^2$. The energy storage proportion of the SC (χ) during the charging process is defined by[33]

$$\chi = E_{SC}/E_{max} \quad (3)$$

An overall conversion efficiency of the integrated device ($\eta_{overall}$) can be obtained by[33]

$$\eta_{overall} = E_{SC}/(P_{in}\times S\times t_{charging}) \quad (4)$$

where P_{in} is the illuminated light density (100 mW cm^{-2}), S is the active area of the solar cell, and $t_{charging}$ is the charging time. The energy storage efficiency of the SC was calculated by[33]

$$\eta_{overall} = \eta_{PSC}\times\eta_{sc} \quad (5)$$

where η_{PSC} is the power conversion efficiency of the PSC.

Supporting Information

The Supporting Information is available free of charge on the ACS Publications website at DOI:...

More results and analysis about PSCs and SCs.

Author Information

Corresponding Author

*E-mail: guanglan.liao@hust.edu.cn (G. Liao).

ORCID

Guanglan Liao: 0000-0002-1849-5473

Notes

The authors declare no competing financial interest.

Acknowledgements

The authors acknowledge the financial support from the National Natural Science Foundation of China (Grant Nos. 51175210 and 51675210), the Program for Changjiang Scholars and Innovative Research Team in University (No. IRT13017), the China Postdoctoral Science Foundation (Grant No. 2016M602283) and the Graduates' Innovation Fund in University (No.

2015650011). We also thank the Analytical and Testing Center of Huazhong University of Science and Technology for the field emission scanning electron microscopy (FESEM).

References

1. Lotsch, B. V. New Light on an Old Story: Perovskites Go Solar. *Angew. Chem. Int. Ed.* **2014**, *53*, 635-637.
2. Park, N.-G. Organometal Perovskite Light Absorbers Toward a 20% Efficiency Low-Cost Solid-State Mesoscopic Solar Cell. *J. Phys. Chem. Lett.* **2013**, *4*, 2423-2429.
3. Snaith, H. J. Perovskites: the Emergence of a New Era for Low-Cost, High-Efficiency Solar Cells. *J. Phys. Chem. Lett.* **2013**, *4*, 3623-3630.
4. Park, N.-G. Perovskite Solar Cells: an Emerging Photovoltaic Technology. *Mater. Today* **2015**, *18*, 65-72.
5. Noh, J. H.; Im, S. H.; Heo, J. H.; Mandal, T. N.; Seok, S. I. Chemical Management for Colorful, Efficient, and Stable Inorganic-Organic Hybrid Nanostructured Solar Cells. *Nano Lett.* **2013**, *13*, 1764-1769.
6. Zhu, W.; Bao, C.; Li, F.; Zhou, X.; Yang, J.; Yu, T.; Zou, Z. An Efficient Planar-Heterojunction Solar Cell Based on Wide-Bandgap $CH_3NH_3PbI_{2.1}Br_{0.9}$ Perovskite Film for Tandem Cell Application. *Chem. Commun.* **2016**, *52*, 304-307.
7. Ogomi, Y.; Morita, A.; Tsukamoto, S.; Saitho, T.; Fujikawa, N.; Shen, Q.; Toyoda, T.; Yoshino, K.; Pandey, S. S.; Ma, T. $CH_3NH_3Sn_xPb_{(1-x)}I_3$ Perovskite Solar Cells Covering Up to 1060 nm. *J. Phys. Chem. Lett.* **2014**, *5*, 1004-1011.
8. Dong, Q.; Fang, Y.; Shao, Y.; Mulligan, P.; Qiu, J.; Cao, L.; Huang, J. Electron-Hole Diffusion Lengths>175 μm in Solution-Grown $CH_3NH_3PbI_3$ Single Crystals. *Science* **2015**, *347*, 967-970.
9. Laban, W. A.; Etgar, L.; Depleted Hole Conductor-Free Lead Halide Iodide Heterojunction Solar Cells. *Energy Environ. Sci.* **2013**, *6*, 3249-3253.
10. Grätzel, M. The Light and Shade of Perovskite Solar Cells. *Nat. Mater.* **2014**, *13*, 838-842.
11. Green, M. A.; Ho-Baillie, A.; Snaith, H. J. The Emergence of Perovskite Solar Cells. *Nat. Photonics* **2014**, *8*, 506-514.
12. Chen, Q.; Zhou, H.; Fang, Y.; Stieg, A. Z.; Song, T.-B.; Wang, H.-H.; Xu, X.; Liu, Y.; Lu S.; You, J. The Optoelectronic Role of Chlorine in $CH_3NH_3PbI_3$(Cl)-Based Perovskite Solar Cells. *Nat. Commun.* **2015**, *6*, 7269.
13. Mei, A.; Li, X.; Liu, L.; Ku, Z.; Liu, T.; Rong, Y.; Xu, M.; Hu, M.; Chen J.; Yang, Y.; Grätzel, M.; Han, H. A Hole-Conductor–Free, Fully Printable Mesoscopic Perovskite Solar Cell with High Stability. *Science* **2014**, *345*, 295-298.
14. Ku, Z.; Rong, Y.; Xu, M.; Liu T.; Han, H. Full Printable Processed Mesoscopic $CH_3NH_3PbI_3/TiO_2$ Heterojunction Solar Cells with Carbon Counter Electrode. *Sci. Rep.* **2013**, *3*, 3132.
15. Xu, X.; Liu, Z.; Zuo, Z.; Zhang, M.; Zhao, Z.; Shen, Y.; Zhou, H.; Chen, Q.; Yang Y.; Wang, M. Hole Selective NiO Contact for Efficient Perovskite Solar Cells with Carbon Electrode. *Nano Lett.* **2015**, *15*, 2402-2408.
16. Wei, H.; Xiao, J.; Yang, Y.; Lv, S.; Shi, J.; Xu, X.; Dong, J.; Luo, Y.; Li, D.; Meng Q.

Free-Standing Flexible Carbon Electrode for Highly Efficient Hole-Conductor-Free Perovskite Solar Cells. *Carbon* **2015**, *93*, 861-868.

17. Li, X.; Tschumi, M.; Han, H.; Babkair, S. S.; Alzubaydi, R. A.; Ansari, A. A.; Habib, S. S. Nazeeruddin, M. K.; Zakeeruddin S. M.; Grätzel, M.; Outdoor Performance and Stability under Elevated Temperatures and Long-Term Light Soaking of Triple-Layer Mesoporous Perovskite Photovoltaics. *Energy Technol.* **2015**, *3*, 551-555.
18. Chen, H.; Wei, Z.; He, H.; Zheng, X.; Wong, K. S.; Yang, S. Solvent Engineering Boosts the Efficiency of Paintable Carbon-Based Perovskite Solar Cells to Beyond 14%. *Adv. Energy Mater.* **2016**, *6*, 1502087.
19. Zhu, Y.; Murali, S.; Stoller, M. D.; Ganesh, K.; Cai, W.; Ferreira, P. J.; Pirkle, A.; Wallace, R. M.; Cychosz K. A.; Thommes, M. Carbon-Based Supercapacitors Produced by Activation of Graphene. *Science*, **2011**, *332*, 1537-1541.
20. Pech, D.; Brunet, M.; Durou, H.; Huang, P.; Mochalin, V.; Gogotsi, Y.; Taberna P.-L.; Simon, P. Ultrahigh-Power Micrometre-Sized Supercapacitors Based on Onion-Like Carbon. *Nature Nanotech.* **2010**, *5*, 651-654.
21. Chmiola, J.; Largeot, C.; Taberna, P.-L.; Simon P.; Gogotsi, Y. Monolithic Carbide-Derived Carbon Films for Micro-Supercapacitors. *Science*, **2010**, *328*, 480-483.
22. Liao, Q.; Li, N.; Cui, H.; Wang, C. Vertically-Aligned Graphene@MnO Nanosheets as Binder-Free High-Performance Electrochemical Pseudocapacitor Electrodes. *J. Mater. Chem. A* **2013**, *1*, 13715-13720.
23. Jiang, J.; Kucernak, A. Electrochemical Supercapacitor Material Based on Manganese Oxide: Preparation and Characterization. *Electrochim Acta* **2002**, *47*, 2381-2386.
24. Peng, Y.; Chen, Z.; Wen, J.; Xiao, Q.; Weng, D.; He, S.; Geng, H.; Lu, Y. Hierarchical Manganese Oxide/Carbon Nanocomposites for Supercapacitor Electrodes. *Nano Res.* **2011**, *4*, 216-225.
25. Wei, W.; Cui, X.; Chen, W.; Ivey, D. G. Manganese Oxide-Based Materials as Electrochemical Supercapacitor Electrodes. *Chem. Soc. Rev.* **2011**, *40*, 1697-1721.
26. Guo, W.; Xue, X.; Wang, S.; Lin, C.; Wang, Z. L. An Integrated Power Pack of Dye-Sensitized Solar Cell and Li Battery Based on Double-Sided TiO_2 Nanotube Arrays. *Nano Lett.* **2012**, *12*, 2520-2523.
27. Xia, X.; Luo, J.; Zeng, Z.; Guan, C.; Zhang, Y.; Tu, J.; Zhang, H.; Fan, H. J. Integrated Photoelectrochemical Energy Storage: Solar Hydrogen Generation and Supercapacitor. *Sci. Rep*. **2012**, *2*, 981.
28. Zhang, X.; Huang, X.; Li, C.; Jiang, H.; Dye-Sensitized Solar Cell with Energy Storage Function Through PVDF/ZnO Nanocomposite Counter Electrode. *Adv. Mater.* **2013**, *25*, 4093-4096.
29. Xue, X.; Wang, S.; Guo, W.; Zhang, Y.; Wang, Z. L. Hybridizing Energy Conversion and Storage in a Mechanical-To-Electrochemical Process for Self-Charging Power Cell. *Nano Lett.* **2012**, *12*, 5048-5054.
30. Xu, J.; Wu, H.; Lu, L.; Leung, S. F.; Chen, D.; Chen, X.; Fan, Z.; Shen, G.; Li, D. Integrated Photo-Supercapacitor Based on Bi-Polar TiO_2 Nanotube Arrays with Selective One-Side Plasma-Assisted Hydrogenation. *Adv. Funct. Mater.* **2014**, *24*, 1840-1846.
31. Chen, T.; Qiu, L.; Yang, Z.; Cai, Z.; Ren, J.; Li, H.; Lin, H.; Sun, X.; Peng, H. An Integrated "Energy Wire" for Both Photoelectric Conversion and Energy Storage. *Angew.*

Chem. Int. Ed. **2012**, *51*, 11977-11980.

32. Miyasaka, T.; Murakami, T. N. The Photocapacitor: an Efficient Self-Charging Capacitor for Direct Storage of Solar Energy. *Appl. Phys. Lett.* **2004**, *85*, 3932-3934.
33. Fu, Y.; Wu, H.; Ye, S.; Cai, X.; Yu, X.; Hou, S.; Kafafy, H.; Zou, D. Integrated Power Fiber for Energy Conversion and Storage. *Energy Environ. Sci.* **2013**, *6*, 805-812.
34. Liang, J.; Zhu, G.; Wang, C.; Wang, Y.; Zhu, H.; Hu, Y.; Lv, H.; Chen, R.; Ma, L.; Chen, T.; Jin, Zhong.; Liu, J. MoS_2-Based All-Purpose Fibrous Electrode and Self-Powering Energy Fiber for Efficient Energy Harvesting and Storage. *Adv. Energy Mater.* **2017**, *7*, 1601208.
35. Xu, X.; Li, S.; Zhang, H.; Shen, Y.; Zakeeruddin, S. M.; Graetzel, M.; Cheng Y.-B.; Wang, M. A Power Pack Based on Organometallic Perovskite Solar Cell and Supercapacitor. *ACS Nano* **2015**, *9*, 1782-1787.
36. Du, P.; Hu, X.; Yi, C.; Liu, H. C.; Liu, P.; Zhang, H. L.; Gong, X. Self-Powered Electronics by Integration of Flexible Solid-State Graphene-Based Supercapacitors with High Performance Perovskite Hybrid Solar Cells. *Adv. Funct. Mater.* **2015**, *25*, 2420-2427.
37. Xu, J.; Ku, Z.; Zhang, Y.; Chao, D.; Fan, H. Integrated Photo-Supercapacitor Based on PEDOT Modified Printable Perovskite Solar Cell. *Adv. Mater. Technol.* **2016**, *1*, 1600074.
38. Zhou, F.; Ren, Z.; Zhao, Y.; Shen, X.; Wang, A.; Li, Y.; Surya, C.; Chai Y. Perovskite Photovoltachromic Supercapacitor with All-Transparent Electrodes. *ACS Nano* **2016**, *10*, 5900-5908.
39. Liu, Z.; Shi, T.; Tang, Z.; Sun, B.; Liao, G. Using a Low-Temperature Carbon Electrode for Preparing Hole-Conductor-Free Perovskite Heterojunction Solar Cells Under High Relative Humidity. *Nanoscale* **2016**, *8*, 7017-7023.
40. Qiu, J.; Qiu, Y.; Yan, K.; Zhong, M.; Mu, C.; Yan, H.; Yang, S. All-Solid-State Hybrid Solar Cells Based on a New Organometal Halide Perovskite Sensitizer and One-Dimensional TiO_2 Nanowire Arrays. *Nanoscale* **2013**, *5*, 3245-3248.
41. Gao, X.; Li, J.; Baker, J.; Hou, Y.; Guan, D.; Chen, J.; Yuan, C. Enhanced Photovoltaic Performance of Perovskite $CH_3NH_3PbI_3$ Solar Cells with Freestanding TiO_2 Nanotube Array Films. *Chem. Commun.* **2014**, *50*, 6368-6371.
42 Wang, G.; Wang, H.; Lu, X.; Ling, Y.; Yu, M.; Zhai, T.; Tong, Y.; Li, Y. Solid-State Supercapacitor Based on Activated Carbon Cloths Exhibits Excellent Rate Capability. *Adv. Mater.* **2014**, *26*, 2676-2682.
43. Raj, C. J.; Kim, B. C.; Cho, W.-J.; Lee, W.-G.; Jung, S.-D.; Kim, Y. H.; Park, S. Y.; Yu, K. H. Highly Flexible and Planar Supercapacitors Using Graphite Flakes/Polypyrrole in Polymer Lapping Film. *ACS Appl. Mater. Interfaces* **2015**, *7*, 13405-13414.
44. Yu, M.; Zeng, Y.; Zhang, C.; Lu, X.; Zeng, C.; Yao, C.; Yang, Y.; Tong, Y. Titanium Dioxide@Polypyrrole Core–Shell Nanowires for All Solid-State Flexible Supercapacitors. *Nanoscale* **2013**, *5*, 10806-10810.
45. Yuan, L.; Lu, X.-H.; Xiao, X.; Zhai, T.; Dai, J.; Zhang, F.; Hu, B.; Wang, X.; Gong, L.; Chen, J. Flexible Solid-State Supercapacitors Based on Carbon Nanoparticles/MnO_2 Nanorods Hybrid Structure. *ACS Nano* **2011**, *6*, 656-661.
46. Lv, Q.; Wang, S.; Sun, H.; Luo, J.; Xiao, J.; Xiao, J.; Xiao, F.; Wang, S. Solid-State Thin-Film Supercapacitors with Ultrafast Charge/Discharge Based on

N-Doped-Carbon-Tubes/Au-Nanoparticles-Doped-MnO_2 Nanocomposites. *Nano Lett.* **2015**, *16*, 40-47.

47. Liu, Y.; Miao, X.; Fang, J.; Zhang, X.; Chen, S.; Li, W.; Feng, W.; Chen, Y.; Wang, W.; Zhang, Y. Layered-MnO_2 Nanosheet Grown on Nitrogen-Doped Graphene Template as a Composite Cathode for Flexible Solid-State Asymmetric Supercapacitor. *ACS Appl. Mater. Interfaces* **2016**, *8*, 5251-5260.
48. Presser, V.; Zhang, L.; Niu, J. J.; McDonough, J.; Perez, C.; Fong, H.; Gogotsi, Y. Flexible Nano-Felts of Carbide-Derived Carbon with Ultra-high Power Handling Capability. *Adv. Energy Mater.* **2011**, *1*, 423-430.
49. Tao, J.; Liu, N.; Ma, W.; Ding, L.; Li, L.; Su, J.; Gao, Y. Solid-State High Performance Flexible Supercapacitors Based on Polypyrrole-MnO_2-Carbon Fiber Hybrid Structure. *Sci. Rep.* **2013**, *3*, 2286.
50. Liu, Z.; Sun, B.; Shi, T.; Tang, Z.; Liao, G. Enhanced Photovoltaic Performance and Stability of Carbon Counter Electrode Based Perovskite Solar Cells Encapsulated by PDMS. *J. Mater. Chem. A* **2016**, *4*, 10700-10709.
51. Zhong, Y.; Shi, T.; Liu, Z.; Huang, Y.; Cheng, S.; Cheng, C.; Li, X.; Liao, G.; Tang, Z. Scalable Fabrication of Flexible Solid-State Asymmetric Supercapacitors with a Wide Operation Voltage utilizing Printable Carbon Film Electrodes. *Energy Technol.* **2017**, *5*, 656-664.
52. Bae, J.; Park, Y. J.; Lee, M.; Cha, S. N.; Choi, Y. J.; Lee, C. S.; Kim, J. M.; Wang, Z. L. Single-Fiber-Based Hybridization of Energy Converters and Storage Units Using Graphene as Electrodes. *Adv. Mater.* **2011**, *23*, 3446-3449.

Novel integrations of perovskite solar cell and supercapacitor based on the carbon electrode are proposed to hybridize energy conversion and storage.

TOC figure